

Effect of Sn and Al additions on the microstructure and mechanical properties of amorphous Ti-Cu-Zr-Ni alloys

Fu-Chuan Chen(陈福川), Fu-Ping Dai(代富平), Xiao-Yi Yang(杨霄熠), Ying Ruan(阮莹), Bing-Bo Wei(魏炳波)

Citation: Chin. Phys. B . 2020, 29(6): 066401 . **doi:** 10.1088/1674-1056/ab8628
Journal homepage: http://cpb.iphy.ac.cn; http://iopscience.iop.org/cpb

What follows is a list of articles you may be interested in

Effect of Ni substitution on the formability and magnetic properties of $Gd_{50}Co_{50}$ amorphous alloy

Ben-Zheng Tang(唐本镇), Xiao-Ping Liu(刘晓萍), Dong-Mei Li(李冬梅), Peng Yu(余鹏), Lei Xia(夏雷)

Chin. Phys. B . 2020, 29(5): 056401 . **doi:** 10.1088/1674-1056/ab7da8

Superhard monoclinic BC_6N allotropes: First-principles investigations

Nian-Rui Qu(屈年瑞), Hong-Chao Wang(王洪超), Qing Li(李青), Yi-Ding Li(李一鼎), Zhi-Ping Li(李志平), Hui-Yang Gou(缑慧阳), Fa-Ming Gao(高发明)

Chin. Phys. B . 2019, 28(9): 096201 . **doi:** 10.1088/1674-1056/ab3439

Secondary relaxation and dynamic heterogeneity in metallic glasses: A brief review

J C Qiao(乔吉超), Q Wang, D Crespo, Y Yang(杨勇), J M Pelletier

Chin. Phys. B . 2017, 26(1): 016402 . **doi:** 10.1088/1674-1056/26/1/016402

Interstitialcy theory of condensed matter states and its application to non-crystalline metallic materials

V A Khonik

Chin. Phys. B . 2017, 26(1): 016401 . **doi:** 10.1088/1674-1056/26/1/016401

Complex force network in marginally and deeply jammed solids

Hu Mao-Bin, Jiang Rui, Wu Qing-Song

Chin. Phys. B . 2013, 22(6): 066301 . **doi:** 10.1088/1674-1056/22/6/066301

Effect of Sn and Al additions on the microstructure and mechanical properties of amorphous Ti–Cu–Zr–Ni alloys*

Fu-Chuan Chen(陈福川), Fu-Ping Dai(代富平)†, Xiao-Yi Yang(杨霄熠), Ying Ruan(阮莹), and Bing-Bo Wei(魏炳波)

Key Laboratory of Material Physics and Chemistry under Extraordinary Conditions of Ministry of Education, Northwestern Polytechnical University, Xi'an 710072, *China*

(Received 26 February 2020; revised manuscript received 31 March 2020; accepted manuscript online 3 April 2020)

Amorphous Ti–Cu–Zr–Ni alloys with minor addition of Sn and Al were prepared by melt spinning technique. The effects of Sn and Al additions on the microstructures and mechanical properties of glassy ribbons were investigated. The amorphous state of ribbons was confirmed by x-ray diffraction and transmission electron microscopy, where those ribbons with Sn addition exhibited a fully amorphous state. The characteristic temperature indicates that $Ti_{45}Cu_{35}Zr_{10}Ni_5Sn_5$ alloy has a stronger glass-forming ability, as proven by differential scanning calorimetry. $Ti_{45}Cu_{35}Zr_{10}Ni_5Al_5$ alloy showed a better hardness of 9.23 GPa and elastic modulus of 127.15 GPa and good wear resistance. $Ti_{45}Cu_{35}Zr_{10}Ni_5Sn_5$ alloy displayed a pop-in event related to discrete plasticity according to nanoindentation. When the temperature is below 560 K, $Ti_{45}Cu_{35}Zr_{10}Ni_5Sn_5$ alloy mainly exhibits elasticity. When the temperature rises between 717 K and 743 K, it shows a significant increase in elasticity but decrease in viscoelasticity after the ribbon experiences the main relaxation at 717 K. When the temperature is above 743 K, the ribbon shows viscoplasticity.

Keywords: metallic glasses, amorphous ribbons, mechanical properties, nanoindentation

PACS: 64.70.Pe, 63.50.Lm, 62.20.–x, 65.60.+a **DOI:** 10.1088/1674-1056/ab8628

1. Introduction

For their specific properties, bulk metallic glasses (BMGs) are fascinating metallic materials that are often not available with traditional crystalline materials.[1] Due to crystalline lattice deletions and defects, such as stacking faults, boundaries, dislocations,[2,3] and the absence of long-range order in the metallic glass, BMGs show a high pressure strength, excellent corrosion resistance behavior, and outstanding soft magnetic properties.[4] Because of their excellent performance, Ti–Cu-based metallic glasses have a broad application prospect in structure and function.[5,6] Nevertheless, metallic glasses are unevenly deformed and have poor plasticity in a narrow shear band.[7,8] To solve this problem, a lot of experiments have been made to enhance plasticity to balance the strength and ductility as required for a component or device.[2,5] It was demonstrated that BMG-based composite materials with different crystal-phase alloying agents could effectively improve the plasticity and processing hardening properties of BMG materials,[9] which blocks the fork or expansion of the shear banding, so that the plastic strains distribution is relatively homogeneous. The plasticity is conspicuously improved.[10]

It is well known that the addition of trace elements also has significant benefits for the mechanical properties and glass-forming ability[9,11] of both BMG composites.[11–13] The alloying elements Fe, Cu, Al, Ni, and Cr can all improve the thermal stability, while the supercooled liquid zone containing Ag and V is narrow in the Ti–Zr–Be ternary alloy.[14] Trace addition of Nb can effectively improve the corrosion resistance of Ti-based amorphous alloys.[15] 0.5-at% Si addition has an optimum glass-forming ability in the $Ti_{42.5}Cu_{42.5}Ni_{7.5}Zr_{7.5}$ alloy,[8] the plasticity increases with the addition of Si without sacrificing their yield strength. To avoid toxic elements such as Be, precious metal elements such as Pd, and brittleness in bulk form, alloying addition effectively crops glass-forming ability[9] and the toughness[16] of BMG-based composite materials. However, it is sporadic to explore the impact of alloying accretion on the mechanical properties and phase formation of BMG composites, although some preliminary experimental results revealed that the damage tolerance and plastic deformation capability of BMG amount of alloying additions.[9] In this research, we compared the glass-forming ability and the mechanical properties of Ti–Cu–Zr–Ni-based amorphous ribbons with Sn or Al element additions. The ribbons were made by a single-roller facility with a water-cooled copper wheel to form Ti–Cu–Zr–Ni amorphous composites with Sn and Al additions. The ribbons are approximately 4-mm wide and 40-μm thick. The thermodynamics and mechanical properties for different ribbons are tested and discussed.

2. Experimental procedures

Master alloy ingots were prepared by arc melting under the atmosphere of Ti-gettered argon, the constituent elements with a higher purity than 99.9%. The master alloy ingots were melted more than three times to ensure uniformity of the com-

*Project supported by the National Natural Science Foundation of China (Grant Nos. 51671161, U1806219, U1660108, and 51327901) and the Research Project of the Natural Science Foundation of Shanxi Province, China (Grant Nos. 2017JM5116 and 2020JZ-08).

†Corresponding author. E-mail: fpdai@nwpu.edu.cn

© 2020 Chinese Physical Society and IOP Publishing Ltd

position. The rapidly solidified melt-spun ribbons were produced by melt spinning technique, in which the master alloy ingots were induction-melted in a quartz tube and then through a nozzle ejected onto a rotating copper wheel surface with high speed in argon atmosphere. The single roller rotation speed is 40 m/s and was cooled internally to ensure amorphous formation. The melt-spun ribbons were about 40-μm thick and 4-mm wide in this work.

The amorphous state of ribbons was verified by x-ray diffractometer (XRD, Rigaku D/max2500 V) using Cu-$K\alpha$ radiation with 2θ angular scanning between 30° and 80° at the sweep speed of 4 °/min. Differential scanning calorimetry (DSC, Netzsch DSC 404C) was carried out to measure the curves of endothermic *versus* temperature from room temperature to 1200 K with a heating rate of 20 K/min in argon atmosphere. According to the endothermic peaks we can get amorphous characteristic temperature, for example the crystallization temperature (T_x) and the glass transition temperature (T_g), *etc*.

The microstructure of the melt-spun ribbons was confirmed by transition electron microscopy (TEM, FEI Talos F200X). TEM is equipped with scanning transmission electron microscopy (STEM) and energy dispersive x-ray spectroscopy (EDX). TEM samples were thinned by ion milling (Gatan 695 PIPS COOL) to make them electron transparent.

Nanoindentation technology has become an effective measuring technique for exploring mechanical characteristics of ribbons under micro-Newton loads, for example the elastic modulus and hardness.[17] To evaluate the mechanical properties, the cross-section of the ribbons was detected by nanoindentation (Hysitron TI980). To ensure accuracy, at least five indents were measured, with the results as the average severity of these tests. Nanoindentation in the load-control mode was made using the Berkovich diamond tip, the maximum applied load is 5 mN, and the loading rate is 1 mN/s. Before the nanoindentation test, samples inlaid with epoxy resin were polished manually using diamond paste. Scanning probe microscopy (SPM, attached by Hysitron TI980) was carried out to observe the surface deformation behavior after nanoindentation.

The dynamic mechanical analysis (DMA) is another extensively used method for investigating mechanical properties.[18,19] Dynamic relaxation processes are related to the mechanical behavior and internal atomic structure of metallic glassy materials,[20] and the procedures were caused by the metastable texture of the amorphous structure. The main relaxation, α relaxation, in glassy materials is interrelated with the viscous flow and the appearance of the glass transition. The mechanical reaction of materials is the sum of three different factors: elasticity, viscoelasticity, and viscoplasticity.[18] Applied periodic stress to the materials,

$$\sigma = \sigma_0 \cos(\omega t), \tag{1}$$

$$\omega = 2\pi f, \tag{2}$$

where ω is the angular frequency, and f is the frequency, record the deformation resulting:

$$\varepsilon = \varepsilon_0 \cos(\omega t + \delta), \tag{3}$$

where δ is the phase lag. The phase lag is directly related to the energy loss generated during the experiment circle.

$$G = \sigma/\varepsilon = G' + \mathrm{i}G''. \tag{4}$$

The formula was used to express the complicated shear modulus of the materials, where G' indicating an elastic response, is called as storage modulus, and G'' is loss modulus, it represents the viscoelastic deformation at low temperatures and viscoplastic deformation at high temperatures or quantities.

$$\tan\delta = G''/G'. \tag{5}$$

The formula links the components of the modulus to phas lag δ. Dynamic mechanical analysis measurements were carried out using DMA-Q800, and the frequency is 1 Hz, and the heating rate is 5 K/min from room temperature to 800 K in this study.

3. Results and discussion

3.1. Effect of alloying on glass-forming ability

The compositions of the synthesized Ti–Cu–Zr–Ni-based melt-spun ribbons are listed in Table 1, including $Ti_{50}Cu_{40}Zr_5Ni_5$ called T0, $Ti_{45}Cu_{35}Zr_{10}Ni_5Al_5$ called T1, and $Ti_{45}Cu_{35}Zr_{10}Ni_5Sn_5$ called T2. Figure 1 shows the typical Ti–Cu–Zr–Ni-based amorphous alloys DSC curves.[8] A glass transition (T_g) accompanied by three exothermic peaks is shown in Fig. 1(a) during the heating process and the heating rate is 20 K/min. The liquidus temperature (T_l) is shown in the high-temperature region as shown in Fig. 1(b). The endothermic characteristic that represents T_g is inconspicuous, so it is difficult to separate a glass transition characteristic out of DSC curves. Because the small area of the supercooled liquid region, the crystallization signal always part or all cover the glass transition signals, and the same situation were observed in aluminum-based bulk metallic glasses.[21] The thermodynamic parameters are listed in Table 2. In addition to T_g, T_x, and T_l, three other values

$$T_{rg} = (T_g/T_l), \tag{6}$$

$$\Delta T_x = (T_x - T_g), \tag{7}$$

$$\gamma_m = (2T_x - T_g)/T_l, \tag{8}$$

where calculated to evaluate the glass-forming ability. Consequently, with the addition of Al, no noticeable enhancement in thermodynamic properties compared to the T0 is observed. At the same time, a higher T_g and T_m and a lower T_l than those of other ribbons took place with the addition of Sn on Ti–Cu–Zr–Ni-based composites. Moreover, the maximum values of T_{rg} and γ_m demonstrate that T2 has a better performance in glass-forming ability.

Table 1. Ti–Cu–Zr–Ni alloys with different components (at.%).

Alloys	Ti	Cu	Zr	Ni	Al	Sn
T0	50	40	5	5	–	–
T1	45	35	10	5	5	–
T2	45	35	10	5	–	5

Table 2. Calorimetric properties of three different alloys.

Alloys	T_g/K	T_x/K	T_l/K	ΔT_x/K	T_{rg}	γ_m
T0	643.4	691.6	1193.9	48.1	0.54	0.62
T1	644.5	686.1	1194.4	41.5	0.54	0.61
T2	671.6	699.3	1153.9	27.7	0.58	0.63

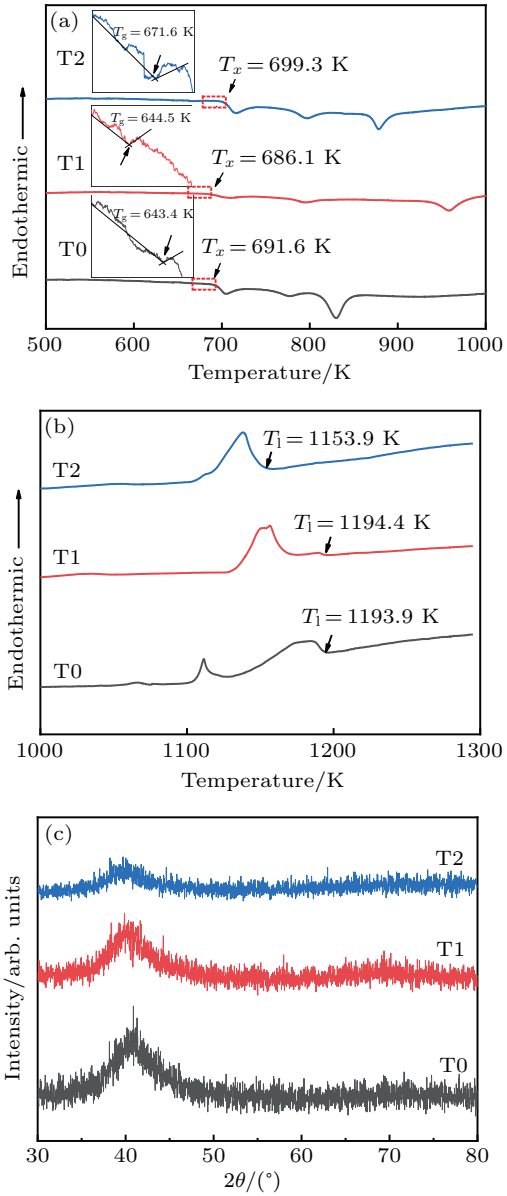


Fig. 1. Characterization of Ti–Cu–Zr–Ni-based alloys: (a) Low- and (b) high-temperature DSC results at a heating rate of 20 K/min, (c) XRD patterns of as-spun ribbons.

Due to the size effect of the atoms,[22] the difference between the atomic radius of the Sn or Al atoms with the alloy system atoms increases the mismatch between the atoms, thereby delaying the long-range arrangement of the atoms required for crystallization, which in turn increases the glass forming ability of the alloy system.[23] On the other hand, due to the negative mixed entropy between the addition elements and the alloy constituent elements,[24] and the mixed entropy of Ti–Sn (-21), Zr–Sn (-43), Ti–Al (-30), and Zr–Al (-44). We know that if there is positive mixed entropy, liquid phase separation will occur. However, research has found that negative mixed entropy can cause nano-scale chemical fluctuations across the entire macro heterogeneity material in the solidification of liquid metal.[25,26] Such fluctuations may enhance the local order of the supercooled liquid,[27] thereby improving the amorphous properties.

3.2. Composition dependence of microstructures

The XRD patterns of the melt-spun ribbons are depicted in Fig. 1(c), revealing a typical amorphous feature. The patterns exhibit only a broad diffraction halo peak between 2θ values of 35° and 45°, meaning the formation of amorphous phase in all the ribbons. No visible sharp Bragg diffraction peaks can be found that correspond to the crystalline structure. However, there are some nanocrystals in the melt-spun ribbon that do not produce clear diffraction peaks, as XRD cannot verify the actual microstructure of nanocrystalline systems with amorphous substrates smaller than 5 nm.[28] To demonstrate this possibility, TEM was used, as presented in Fig. 2, showing the coexistence of crystalline and amorphous states.

The T0 ribbons corresponding TEM graphs and selected area diffraction (SAED) patterns are shown in Figs. 2(a) and 2(b). For T0, heterogeneously distributed nanocrystallites exist in the amorphous matrix. In parallel, amorphous and crystalline phases coexist in the T0 alloy, as evidenced by the diffraction points and diffuse halo rings in the SAED pattern (b). More details of the image in Fig. 2(c) are given with a higher resolution. The lattice fringes area indicates that the crystalline structure can be observed clearly in the circled area.

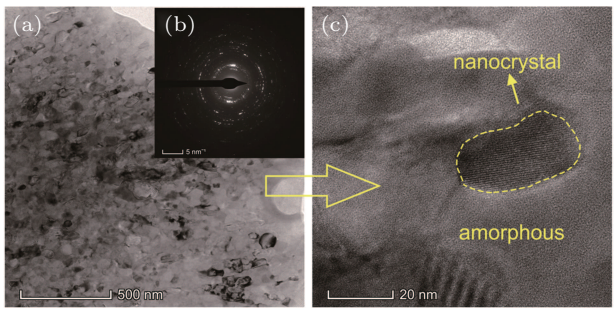


Fig. 2. Microstructures of quaternary $Ti_{50}Cu_{40}Zr_5Ni_5$ alloy: (a) TEM images, (b) SAED patterns, (c) details of nanocrystals.

For T1 as shown in Fig. 3, we can still see the coexistence of crystalline and amorphous phases according to the

SAED pattern in Fig. 3(b). Nevertheless, the TEM image of T2 (Fig. 4) display more homogeneously distributed nanocrystallites than T1. In contrast, the featureless contrast and wide halo ring indicate a fully amorphous structure, as shown in Fig. 4(b). Simultaneously, the elemental allocation in the T1 and T2 ribbons was investigated by EDX and present the homogeneity of the T1 and T2 ribbons, their chemical composition was determined by EDX analysis, as shown in Figs. 3(c)–3(g) and 4(c)–4(g).

Additionally, theb atomic segregation has not been found,[1] and the as-spun ribbons displayed a uniform atomic allocation in the mappings. It is worth while noting that the chemical homogeneity is identical for both T1 and T2 ribbons. On the other hand, the concentrations of Ti and Cu are higher than those of other elements due to the compositions of the ribbon.

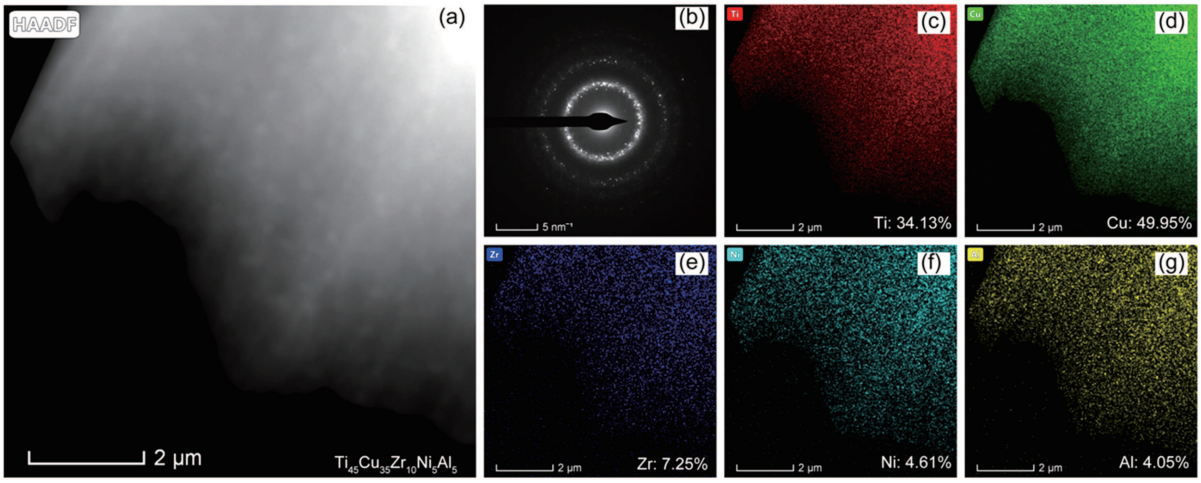


Fig. 3. Microstructures of quinary $Ti_{45}Cu_{35}Zr_{10}Ni_5Al_5$ alloy: (a) STEM image, (b) SAED patterns, and EDX mappings (c)–(g).

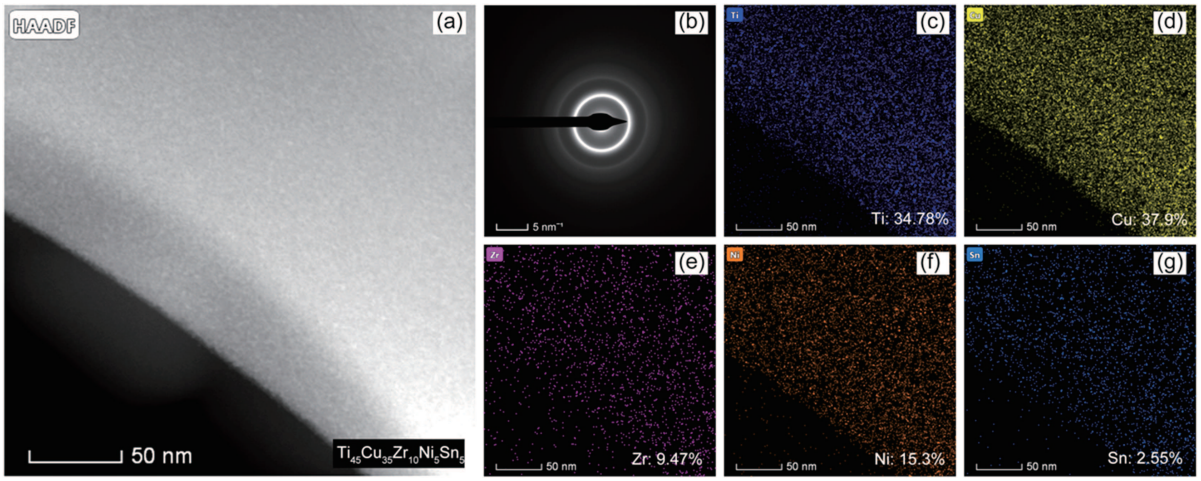


Fig. 4. Microstructures of quinary $Ti_{45}Cu_{35}Zr_{10}Ni_5Sn_5$ alloy: (a) STEM image, (b) SAED patterns, and EDX mappings (c)–(g).

3.3. Mechanical properties of amorphous alloys

Nanoindentation is an applicable apparatus to characterize the mechanical properties of the ribbons. In this work, the indentation function, a total of 12 s, the loading process is 5 s to 5 mN, maximum force is maintained at 2 s, and 5 s are finally unloaded as depicted in Fig. 5(a). The representative load *versus* displacement curves, which is so called *P*–*h* curves, got from the Berkovich indentations on the alloys are illustrated in Figs. 5(b)–5(d) under the same experimental conditions corresponding to T0, T1, and T2, respectively. For the T2 curve (Fig. 5(d)), the typical pop-in event, which is a symbol of discrete plasticity,[29] can be conspicuously observed in the insets, showing the enlargements of the circled area. As widely reported in metallic glass materials, the pop-in events are related to the shaping and expansion of shear bands.[30] This phenomenon was also detected in Ti-rich[31] and Al-rich[21] metallic glasses. The pop-in events in T0 insets Fig. 5(b) and T1 insets Fig. 5(c) indicate that shear band activity is not as remarkable as that of T2 in alloy plastic deformation.

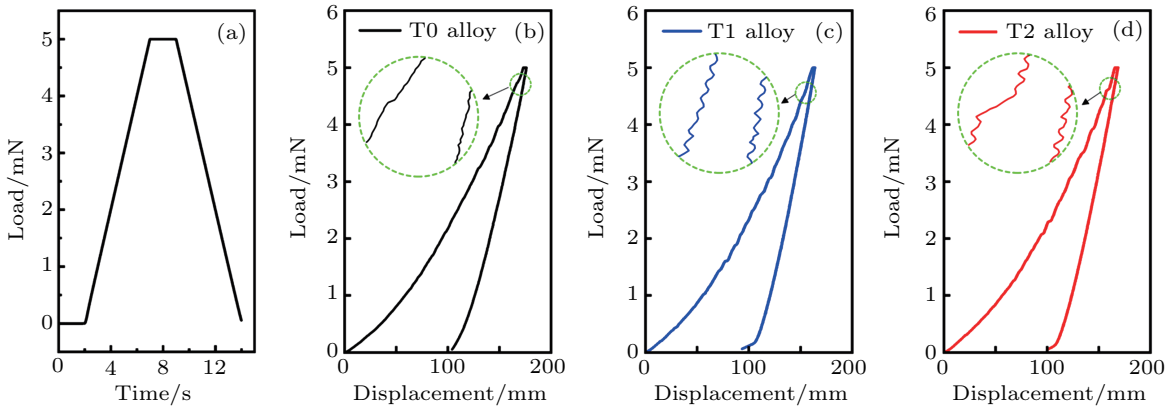


Fig. 5. Nanoindentation properties of three amorphous alloys: (a) the load–time curve, (b) $Ti_{50}Cu_{40}Zr_5Ni_5$, (c) $Ti_{45}Cu_{35}Zr_{10}Ni_5Al_5$, and (d) $Ti_{45}Cu_{35}Zr_{10}Ni_5Sn_5$. The circled insert corresponds to the typical pop-in event.

The hardness (H) and reduced elastic (Young's) modulus (E_r) values were counted based on the Oliver and Pharr method[17] from the P–h curves and are summarized in Fig. 6(a). According to the indentation curves unloading portion gradient, E_r was determined. As a result, the hardness increased linearly with the addition of Sn and Al to the T0 matrix, which showed the hardness of 9.23 GPa was observed for T1. T2 exhibits a moderate hardness of 8.84 GPa. The Young's modulus demonstrates the same regularity with hardness, with the values of 101.59 GPa, 127.15 GPa, and 119.76 GPa corresponding to T0, T1, and T2, respectively. Generally, an increase in the reduced elastic modulus E_r was accompanied by an increase in the hardness H. Hence, the consequence suggested that T1 exhibits the best performance in hardness and Young's modulus characteristics.

In addition to hardness and Young's modulus, nanoindentation contributes to the acquisition of other significant indicators to forecast the working life of devices or equipment.[32] In principle, metallic glasses are supposed to display excellent wear resistance as a result of high strength and grain boundaries missing.[33] According to the measurement results of nanoindentation, it is widely reported that that the wear resistance of the alloy is positively correlated with the H/E_r ratio, which has been widely reported.[32,34,35] Generally, our results reveal the nearly identical wear resistance according to the H/E_r ratio, as shown in Table 3. Another indicator connected with the wear property is H^3/E_r^2. When in loaded contact, H^3/E_r^2 is proportional to the impedance of the materials to plastic deformation.[36] This substantially stands for the grater the impedance to plastic deformation is, the ratio H^3/E_r^2 higher is. The value of H^3/E_r^2 ratio displayed a prominent regularity, which reveals that T1 and T2 have better resistance to plastic deformation than T0 without element addition. Overall, the trace addition of Sn and Al elements exhibited optimized performance in wear resistance, as seen by comprehensively evaluating the two parameters. Currently, nanoindentation is increasingly used to detect the metallic glassy materials deformation behavior. The further plastic deformation is limited to a few amounts of material near the indentation.[37] To further describe the typical surface deformation features, SPM observations around the indents were investigated in T0. Figure 6(a) insets show the 3D morphology of the usual impression marks of T0 after a maximum load of 5 mN, the standard pileup was observed in topographic profile after nanoindentation. The cooling rate during ribbon fabrication has a significant infection on the pileup, and the cooling rate is related to the material flow during plastic deformation of the ribbons.[31]

Table 3. The H/E_r and H^3/E_r^2 values of three amorphous alloys.

Alloys	H/E_r	H^3/E_r^2
T0	7.56×10^{-2}	4.38×10^{-2}
T1	7.26×10^{-2}	4.86×10^{-2}
T2	7.38×10^{-2}	4.82×10^{-2}

Besides, T2 exhibited fascinating properties in the above mentioned investigation. Furthermore, DMA is a widely used method to explore the mechanical properties of T2. Figure 6(b) exhibits the temperature *versus* the loss modulus (G''), the storage modulus (G'), and the phase lag δ of T2, the loading frequency is $\omega = 1$ Hz and the heating rate is 5 K/min. Consequently, the typical dynamic mechanical behavior of T2 can be segmented into three areas. Area (I): When the temperature is inferior to 560 K, G' is nearly constant 36 GPa, whereas G'' is constant at approximately 0.5 GPa, which indicates the amorphous state of the ribbon. Therefore, the ribbon exhibits strongly elastic properties, but the viscoelasticity nature is negligible at low temperatures. With the temperature increased to 685 K, the G' reached the highest value of 46.7 GPa, and G'' begin to raising, indicating the increase of viscoelasticity. Area (II): G'' arrived a maximum amount of 10 GPa at a temperature of 717 K, which is called T_α and is associated with the main relaxation, α relaxation, meaning the appearance of the dynamic glass transition.[38] The outright increase in G'' and the decrease in G' in Area (II) indicate a marked rise in elasticity but decrease in viscoelasticity after the ribbon experiences α relaxation. Area (III): In contrast, the storage modulus decreases, nevertheless the loss modulus increases after 743 K as a result of crystallization, the ribbon

indicates viscoplasticity. The internal friction ($\tan\delta$) displays a similar tendency to loss modulus during the whole process; nevertheless, a small difference is observed in T_α because of the dramatically reduced G' in this area.

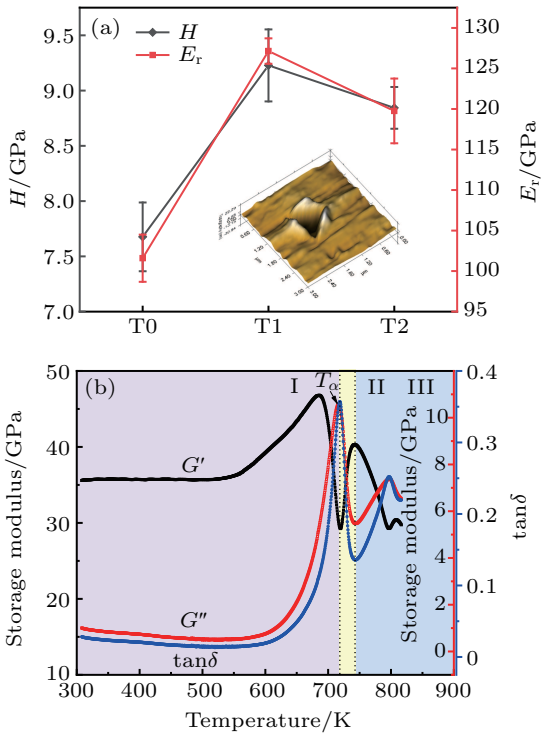


Fig. 6. Mechanical properties of amorphous alloys: (a) the hardness (H) and reduced Young's modulus ($E_{r)}$ curves, (b) the the storage modulus (G'), loss modulus (G''), and internal friction ($\tan\delta$) of $Ti_{45}Cu_{35}Zr_{10}Ni_5Sn_5$.

4. Conclusions

The comparative study of the thermodynamics and mechanical properties of Ti–Cu–Zr–Ni melt-spun ribbons with Sn and Al addition were investigated in this paper. Our results reveal that the addition of Sn can improved the amorphous formation ability of the Ti–Cu–Zr–Ni ribbons more than that of Al. With the addition of Sn, the homogeneous distribution of characterless contrast in the microstructure of $Ti_{45}Cu_{35}Zr_{10}Ni_5Sn_5$ reveals the totally amorphous state. On the other hand, there is a conspicuous enhancement in the mechanical properties upon trace addition of Sn and Al. Furthermore, the addition of Al results in a higher hardness, elasticity and excellent wear resistance. $Ti_{45}Cu_{35}Zr_{10}Ni_5Sn_5$ shows the discrete plasticity by the pop-in event in nanoindentation. The ribbons display strong elasticity at a low temperature and experience a noticeable increase in elasticity but a decrease in viscoelasticity after α relaxation. The viscoplasticity plays a main role after 743 K.

Acknowledgments

The authors wish to acknowledge Dr. W Löser, Prof. J He, Prof. Z J Yan and Prof. K K Song for their helpful discussions.

References

[1] Borja C E, Figueroa I A, Lozada-Flores O, Estrada M, Lara-RodrÍGuez G A and Verduzco J A 2018 *Trans. Nonferrous Met. Soc. Chin.* **28** 1157
[2] Gargarella P, Pauly S, Samadi Khoshkhoo M, Kühn U and Eckert J 2014 *Acta Mater.* **65** 259
[3] Sun D, Shang C, Liu Z and Gong X 2017 *Chin. Phys. Lett.* **34** 026402
[4] Sun Y T, Wang C, Lu Y M, Hu Y C, Luo P, Liu M, Xian H J, Zhao D Q, Ding D W, Sun B A, Pan M X, Wen P, Bai H Y, Liu Y H and Wang W H 2018 *Acta Phys. Sin.* **67** 126101 (in Chinese)
[5] Inoue A and Takeuchi A 2011 *Acta Mater.* **59** 2243
[6] Fornell J, Van Steenberge N, Varea A, Rossinyol E, Pellicer E, Surinach S, Baro M D and Sort J 2011 *J. Mech. Behav. Biomed. Mater.* **4** 1709
[7] Greer A L 2009 *Materials Today* **12** 14
[8] Gargarella P, Pauly S, Khoshkhoo M S, Kiminami C S, Kühn U and Eckert J 2016 *J. Alloys Compd.* **663** 531
[9] Zhang Z Y, Wu Y, Zhou J, Song W L, Cao D, Wang H, Liu X J and Lu Z P 2013 *Intermetallics* **42** 68
[10] Hofmann D C, Suh J Y, Wiest A, Duan G, Lind M L, Demetriou M D and Johnson W L 2008 *Nature* **451** 1085
[11] González S 2016 *J. Mater. Res.* **31** 76
[12] Liu Z Q, Li R, Liu G and Su W H 2012 *Acta Mater.* **60** 3128
[13] Kolodziejska J A, Kozachkov H, Kranjc K, Hunter A, Marquis E, Johnson W L, Flores K M and Hofmann D C 2016 *Sci. Rep.* **6** 22563
[14] Gong P, Wang X and Yao K 2016 *J. Mater. Sci.* **51** 5321
[15] Wu X W, Zhou Y, Chen F and Qin F X 2019 *Mater. Sci. Technol.* **27** 73 (in Chinese)
[16] Garrett G R, Demetriou M D, Chen J and Johnson W L 2012 *Appl. Phys. Lett.* **101** 241913
[17] Oliver W C and Pharr G M 1992 *J. Mater. Res.* **7** 1564
[18] Qiao J C and Pelletier J M 2014 *J. Mater. Sci. Technol.* **30** 523
[19] Wang Q, Pelletier J M and Blandin J J 2010 *J. Alloys Compd.* **504** 357
[20] Kong J, Ye Z, Chen W, Shao X, Wang K and Zhou Q 2015 *Mater. Des.* **88** 69
[21] Guo H, Jiang C, Yang B and Wang J 2017 *J. Mater. Sci. Technol.* **33** 1272
[22] Egami T and Waseda Y 1984 *J. Non-Cryst. Solids* **64** 113
[23] Wang W H 2007 *Prog. Mater. Sci.* **52** 540
[24] Takeuchi A and Inoue A 2005 *Mater. Trans.* **46** 2817
[25] Yao K F, Ruan F, Yang Y Q and Chen N 2006 *Appl. Phys. Lett.* **88** 122106
[26] Guan P F, Wang B, Wu Y C, Zhang S, Shang B S, Hu Y C, Su R and Liu Q 2017 *Acta Phys. Sin.* **66** 176112 (in Chinese)
[27] Sheng H W, Luo W K and Alamgir F M 2006 *Nature* **439** 419
[28] Venkataraman S, Stoica M, Scudino S, Gemming T, Mickel C, Kunz U, Kim K B, Schultz L and Eckert J 2006 *Scr. Mater.* **54** 835
[29] Medeiros B B, Medeiros M M, Fornell J, Sort J, Baró M D and Jorge A M 2015 *J. Non-Cryst. Solids* **425** 103
[30] Aliaga L C R, Jordina F B, Suriñach S, Baró M D, Kiminami C S, Bolfarini C, Botta W J and Sort Viñas J 2013 *J. Mater. Res.* **28** 2740
[31] Huang Y, Chiu Y L, Shen J, Chen J J J and Sun J 2009 *J. Alloys Compd.* **479** 121
[32] Fornell J, González S, Rossinyol E, Suriñach S, Baró M D, Louzguine-Luzgin D V, Perepezko J H, Sort J and Inoue A 2010 *Acta Mater.* **58** 6256
[33] Bhatt J, Kumar S, Dong C and Murty B S 2007 *Mater. Sci. Eng.: A* **458** 290
[34] Leyland A and Matthews A 2000 *Wear* **246** 1
[35] Rebholz C, Leyland A, Schneider J M, Voevodin A A and Matthews A 1999 *Surf. Coat. Technol.* **120-121** 412
[36] Musil J, Kunc F, Zeman H and Pola´kova H 2002 *Surf. Coat. Technol.* **154** 304
[37] Kim J J, Choi Y, Suresh S and Argon A S 2002 *Science* **295** 654
[38] Qiao J C and Pelletier J M 2014 *J. Alloys Compd.* **589** 263